



Indian Institute of Technology Bombay

EE451 : Supervised Research Exposition
2022-23/I

Analyzing the characteristics of Type-II
Structures for Infrared Applications

Mayur Ware

19D070070

4th-year Dual Degree Student in Electronic Systems Specialization
Department of Electrical Engineering, IIT Bombay

Guided by :

Prof. Subhananda Chakrabarti

Department of Electrical Engineering, IIT Bombay

Final Report

November 22, 2022

Index

1. Learning Phase	...3
2. Simulation - I	...13
Mid-Wave Infrared InAs/GaSb Type-II Superlattice Photodetector With n-B-p Design Grown on GaAs Substrate	
3. Simulation - II	...19
Hybrid Type-II GaSb/GaAs Quantum Dot Structure	
4. Appendix	...24
5. References	...24

1. Learning Phase

Optical detectors or photodetectors are electromagnetic sensors that convert electromagnetic radiation into electric signals that can be measured through an appropriate device. Thus, the output electric signal is proportional to the incident light or electromagnetic radiation. They play a significant role in telecommunication systems.

In recent times, photodetectors in optical/telecommunication with Si based chips have attracted the industry for operations in visible spectral range. However, because of the higher bandgap of Si as compared to infrared photon, it is not suitable for the telecommunication spectrum ($1.3\text{-}1.6 \mu\text{m}$). To overcome this issue, Ge-based photodetectors are used for telecommunication region due to its lower bandgap. But, there is another disadvantage associated with it due to thermal mismatch stress and costly processes. Thus, use of conventional Quantum Dots based Infrared Photodetectors (QDIPs) is not very feasible due to such complexity. So, research progressed to find an alternative.

Modern research methods have found an alternative in type-II superlattice photodiodes. Type-II SuperLattice (T2SL) is also referred as Strained Layer Superlattice (SLS). It is a technology that can be used to make high-quality cooled IR photodetectors with cut-off wavelength ranging from $2\mu\text{m}$ to $30\mu\text{m}$ which covers all kinds of wavelength bands. In this report, I'll try to summarize my studies related to these topics.

Mercury Cadmium Telluride (MCT) :

The very first IR detector was based on PbS which could detect up to $3\mu\text{m}$ wavelength. The detection spectrum was later extended using PbSe, PbTe, InSb and new semiconductor alloy materials such as Mercury Cadmium Telluride (MCT).

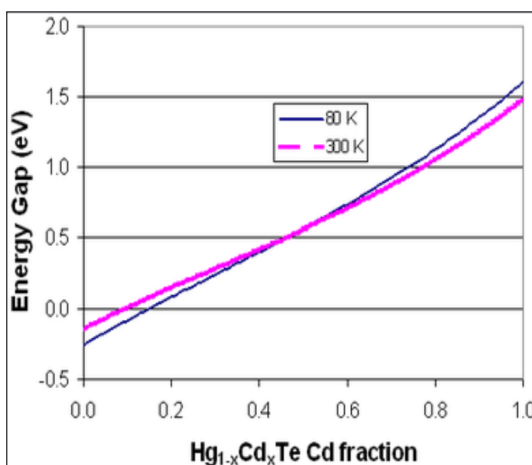


Figure 1
Reference : [10]

Mercury Cadmium Telluride (Hg_{1-x}Cd_xTe) is a chemical compound with a tunable bandgap spanning the shortwave infrared (SWIR) to very long wave infrared regions (VLWIR). The amount of cadmium (Cd) in the alloy can be chosen so as to tune the optical absorption of the material to the desired infrared wavelength. CdTe is a semiconductor with a bandgap of approximately 1.5 eV at room temperature. HgTe is a semimetal, which means that its bandgap energy is zero. Mixing these two substances allows one to obtain any bandgap between 0 and 1.5 eV. MCT technology is grown on ZnCdTe and has some uniformity and dark current issues.

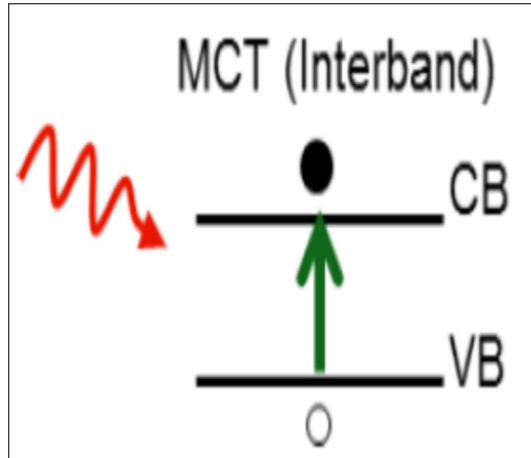


Figure 2
Reference : [3]

Quantum Well Infrared Photodetectors (QWIPs) :

Quantum Well Infrared Photodetectors (QWIP) are one of the simplest quantum mechanical device structures that can detect MWIR and LWIR radiation spectrum. They are known for their stability, high pixel-to-pixel uniformity, and high-pixel operability.

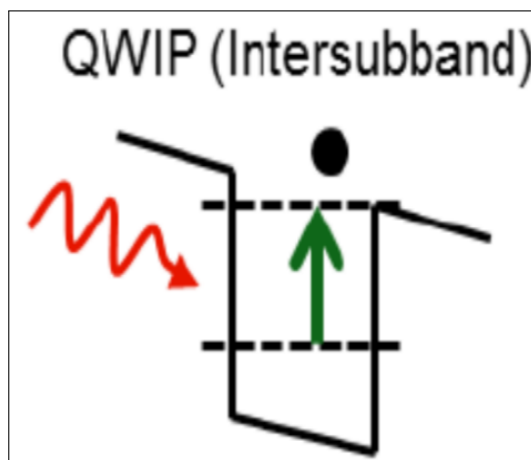


Figure 3
Reference : [3]

In QWIPs, AlGaAs/GaAs QWs are grown GaAs substrates. QWIPs offer better uniformity but poor quantum efficiency over MCT. Depending on the material and the design of the quantum wells, the energy levels of the QWIP can range between 3 to $20\mu\text{m}$.

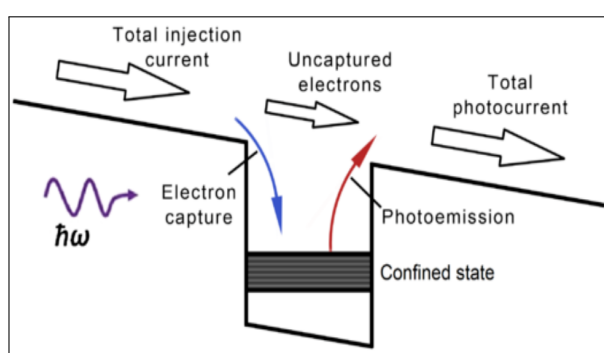


Figure 4
Reference : [10]

To balance the loss of electrons from the quantum well, electrons are injected from the top emitter contact. Since the capture probability is smaller than one, extra electrons need to be injected and the total photocurrent can become larger than the photoemission current.

Quantum Dot Infrared Photodetectors (QDIPs) :

In QDIPs, nanometer size features of one semiconductor material grown on other material are known

as Quantum dots. Generally, InAs dots are grown on GaAs substrate. QDIP is the next level innovation after MBE and its application is mainly in the focal plane arrays (FPAs). Quantum dots are formed by the release of compressive strain when the thickness of the film exceeds critical thickness. Layer-by-layer 2-D patterns are used to form 3-D island growth. These QDIPs are similar to QWIPs but quantum wells are replaced by quantum dots.

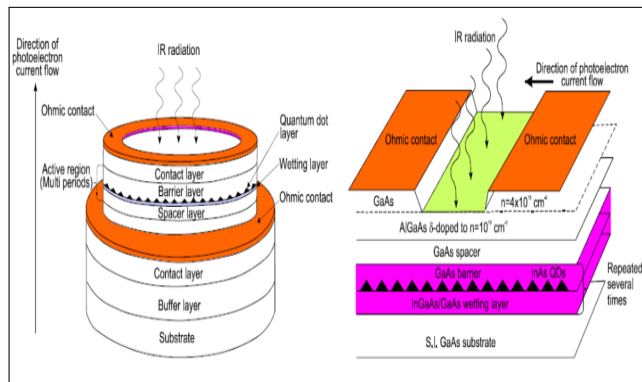


Figure 5
Reference : [2]

Conventional (vertical) and lateral are the two types of QDIP structures shown in Fig. 5. Wavelength change is engineered by adjusting quantum well size and structure.

QD confinement barriers are created in the conduction and valence bands and hence, they provide a mechanism for quantum confinement in addition to the nanoscale size of QDs. Fig. 6 shows the energy band diagram of InAs QDs on GaAs. Free electrons are provided by doping Si.

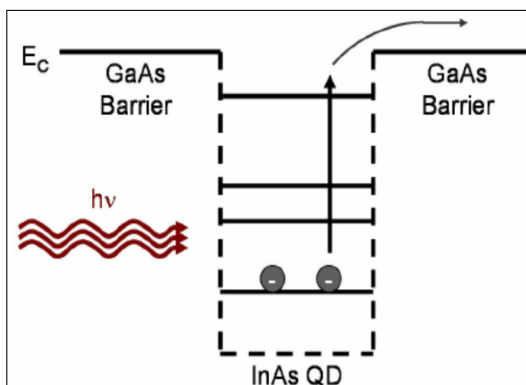


Figure 6
Reference : [8]

The structure shown in Fig. 7 is the standard InAs/GaAs QDIP device heterostructure which comprises of an active region with top and bottom doped n-type contact layers. In the active region, 10-30 QD InAs layers are separated by large GaAs barriers to avoid strain propagation.

Currently, the Stranski-Krastanow (S-K) growth mode is the most successful approach to achieve defect-free, multiple-layer and high-density QDs. The thickness of GaAs cap layer is 25-60nm.

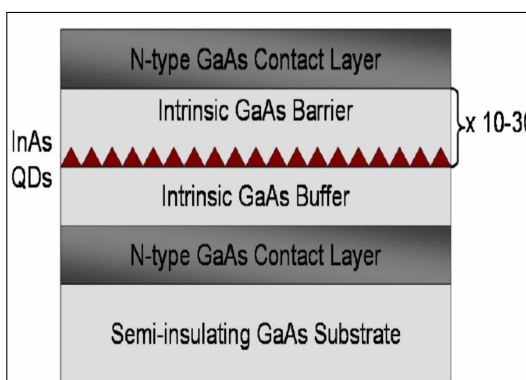


Figure 7
Reference : [8]

There are two type of intraband transitions observed on these QDs :

i) ground state to excited state

ii) ground or excited to the continuum of energy levels near the band edge.

Generally, the QD absorption spectrum is broad due to size variations which deteriorates QDIP performance, especially due to dark current. Absorption efficiency and dark current also depend on dopant densities where higher dopant density increases dark current and lower dopant density decreases absorption efficiency.

AlGaAs is advantageous as a barrier material due to its larger bandgap that helps reduce dark current.

The boron doped devices use holes trapped in the QD valence band for the photogeneration of carriers play an important technology for far IR detection.

InAs QDs embedded in strain-relieving InGaAs quantum wells are called as DWELL heterostructures.

QDIPs using DWELL such as InAs/In_{0.15}Ga_{0.85}As not only permit greater control over detection wavelength tunability and also demonstrated excellent device performance.

Advantages of QDIPs over QWIPs :

i) Normal incidence absorption is observed in QDIPs whereas, in QWIPs, have to be perpendicular only.

ii) Signal to noise ratio of QDIPs is significantly high as compared to QWIPs mainly due to lower thermal generation of electrons.

iii) Lower dark current in QDIPs due to well confined 3-D alignment. Although, a major issue in QDIP is variation in dot size which results in degradation of the absorption coefficient. Detectivity decreases with increase in temperature. The performance of a very uniform QDIP is comparable with HgCdTe photodetectors.

Colloidal QDIPs :

A different approach is used where nanoparticles are synthesized by inorganic chemistry and these nanoparticles are called as colloidal QDIPs. They could improve performance as compared to epitaxial QDs due to :

i) more control over size-filtering leads to uniform QDs

ii) spherical shape of QDs

iii) greater selection of active region materials.

Fig. 8 is a schematic diagram of a colloidal heterostructure.

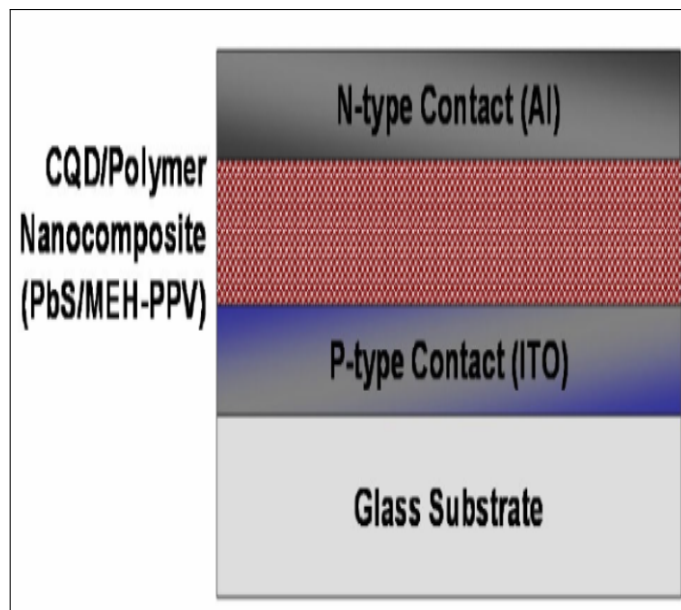


Figure 8
Reference : [8]

The IR photodetection mechanism is explained in the energy spectrum where colloidal QDs are electron acceptors and the polymers are typically hole conductors. Hence, photoconduction through the nanocomposite occurs as electrons hop among QDs and holes transport through the polymer.

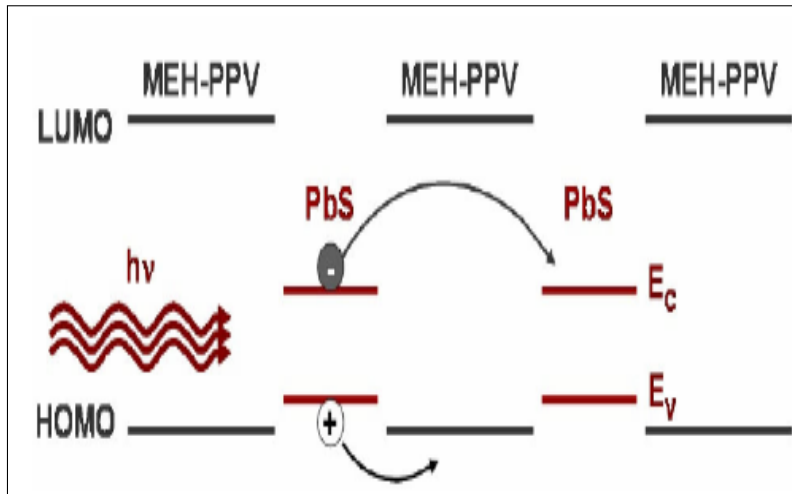


Figure 9
Reference : [8]

Photoluminescence studies of QDs :

In Glaser et al [6], PL studies are performed on 3 ML InSb, 3 ML GaSb and 4 ML AlSb S-K grown QDs. As compared to GaAs, lattice constants of InSb, GaSb and AlSb are 14.6%, 7.8% and 8.5% larger, respectively. QDs are immediately formed after the initial growth of 3 ML layers. To observe the PL of these quantum structures, a thin GaAs cap layer is deposited.

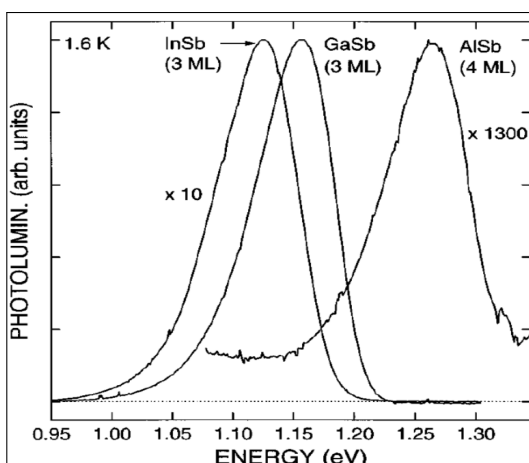


Figure 10
Reference : [6]

Fig. 10 shows the PL spectra obtained at 1.6K from 3 ML InSb, 3 ML GaSb and 4 ML AlSb QDs. The width of these PL curves is due to the convolution of emission from QDs of different sizes.

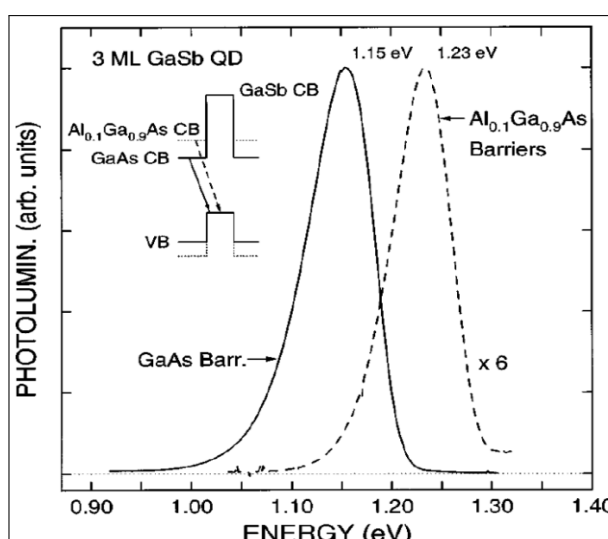


Figure 11
Reference : [6]

In Fig. 11, a comparison is made between PL curves from 3 ML GaSb QDs grown on GaAs and $\text{Al}_{0.1}\text{Ga}_{0.9}\text{As}$ barrier layers. It is observed that the peak energy of 3 ML GaSb QDs grown on $\text{Al}_{0.1}\text{Ga}_{0.9}\text{As}$ the substrate is shifted by 80meV as compared to GaAs substrate. It is due to changes in confinement energies due to the expected heavy mass of holes in the GaSb QDs.

Type-II SuperLattice (T2SL) :

A system made of a repeating sequence of thin layers of different materials is known as a superlattice. If both the valence and the conduction band edge of the second material are above the band edges of the first material, it is called a broken type II band alignment.

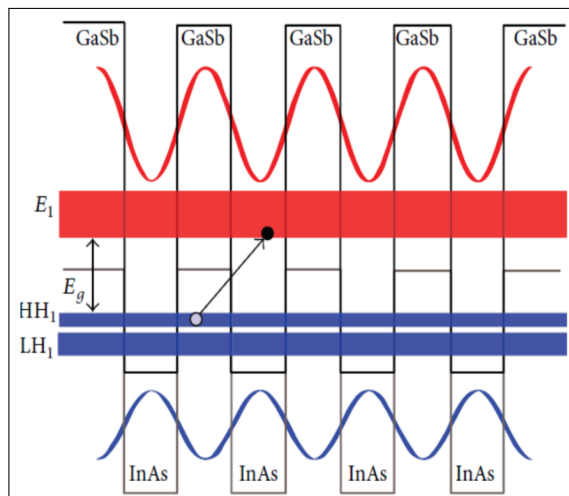


Figure 12
Reference : [1]

Electron and hole wavefunctions in InAs and GaSb of InAs/GaSb T2SL respectively are shown in Fig. 12. The operating range of this Type-II Superlattice Photodetector (T2SL) can be varied by varying the thickness of these layers. Several techniques such as Mobility Spectrum Analysis (MSA) are used to measure and analyze the electrical properties. The performance of T2SL devices strongly depends on structural perfection, interfacial roughness, etc. The high conversion quantum efficiency of T2SL is better than QWIPs. Though, the dark current density in T2SL is significantly higher than in MCT detectors. The SRH and thermally generated diffusion currents may be significantly reduced by the exclusion of the GaSb layer from InAs/GaSb T2SL stack.

It is a high-performance material used recently in IR detectors in MWIR and LWIR range. It consists of repeated monolayers of InAs and GaSb. InAs layers experience tensile strain due to lattice mismatch. Bandgap can be varied by changing the composition and thickness of monolayers. Dark current is a major issue that has two components, bulk leakage and surface leakage. They depend on the material quality and device fabrication respectively. A proper etching and sidewall passivation is used to improve surface leakage. Whereas, the use of GaAs as substrate reduces cost.

It is a QD method with type-II band alignment. The conduction band of matrix material is at lower energy than the valence band of dot (QD) material. Holes are trapped in quantized energy states whereas electrons are free to move in the conduction band.

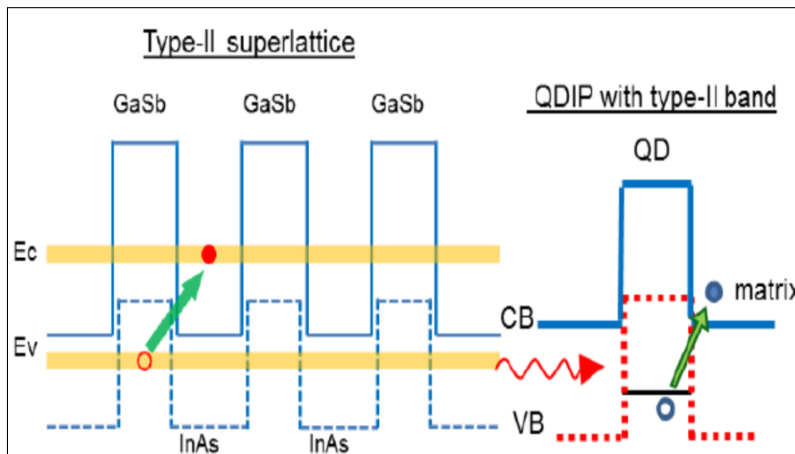


Figure 13
Reference : [3]

GaAs QDs on InAs and InSb QDs on InAs are some combinations used where GaAs dots on InAs are tensely strained and InSb dots on InAs are compressively strained. Larger dots cause a red shift in the spectrum and vice versa.

Advancements in T2SL :

I) 'M' Structure Type-II Photodetectors :

A modification is done in pre-existing type-II superlattice system to make it a type-II M superlattice. A thin film of AlSb is inserted in the middle of the GaSb layer in normal type-II InAs/GaSb superlattice. The figure alongside shows the energy band diagram of type-II M superlattice. The AlSb barrier reduces the dark current.

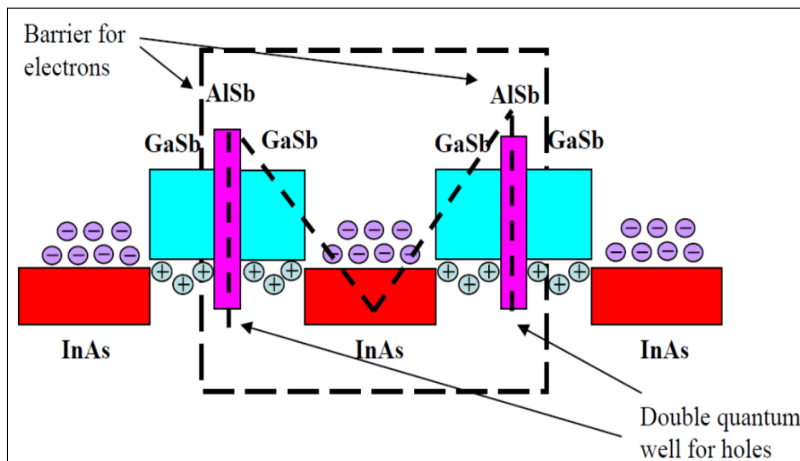


Figure 14
Reference : [4]

The effective mass of electrons increases with an increase in the number of monolayers which decreases their mobility and blocks dark currents. Along with a thick GaSb superlattice, the AlSb layer provides a positive impact on electron-hole confinement which enhances the optical properties of this material. By inserting AlSb barrier in GaSb layer, the thickness of GaSb is reduced and two quantum wells for holes are created which results in better optical properties. As shown in the Fig. 15, the first valence band (V1) moves upward while the second valence band level (V2) remains unchanged as we increase the thickness of the AlSb barriers. At a certain thickness of AlSb, these two bands coincide.

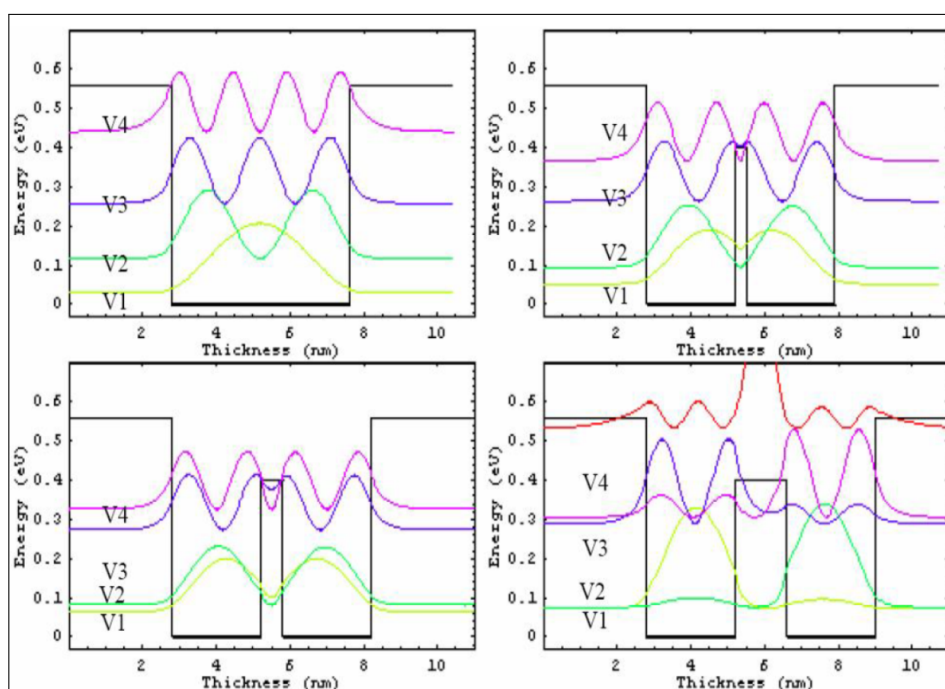


Figure 15
Reference : [4]

II) T2SL with n-B-p design :

To tackle the dark current issue in the conventional p-i-p architecture of InAs/GaSb type-II superlattice, various heterostructures such as n-B-n, n-B-p and complementary p-B-i-B-n designs which utilize the engineering freedom of band structure. GaAs substrate offers more advantages compared to GaSb but its layers are highly mismatched. In these structures, most of the depletion electric field drops across the wide bandgap barrier layer, reducing the dark current.

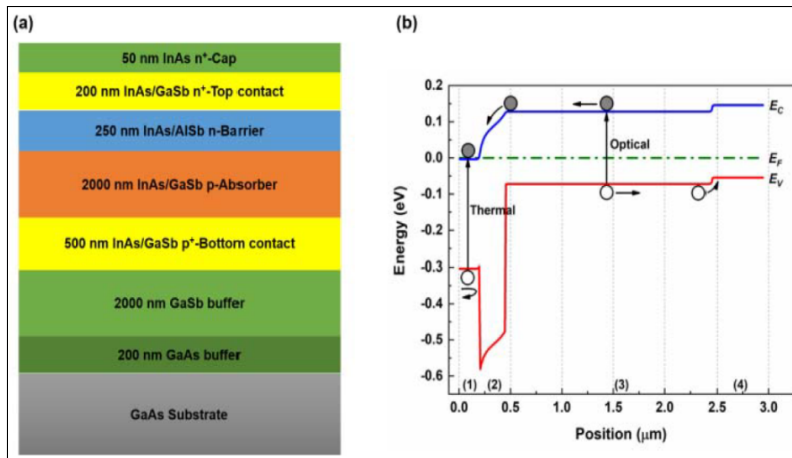


Figure 16

Reference : [5]

Optical and Thermal transitions are associated with photocurrent and dark current respectively. In n-B-n design, the photocurrent is based on minority holes whereas in n-B-p design, the p-doped absorber enables the higher mobility electrons to be the minority photocarriers, which is capable to attain higher quantum efficiency.

III) Radiactive recombination in T2QDs :

Uniform layers of strained coherent islands can be formed using self-organizing effects in the S-K growth. In the GaSb/GaAs system, after depositing a certain number of GaSb MLs, 3-D GaSb QDs on GaAs are formed. TEM studies show that well-resolved GaSb dots are formed starting at approximately 1.2 nm GaSb deposition. These QDs are rectangular in shape with size of 20nm.

Fig. 17 shows band energy structure of completely relaxed and pseudomorphic (compressively strained) GaSb/GaAs heterostructures. Conduction band in the pseudomorphic structure is increased sharply due to compressive strain.

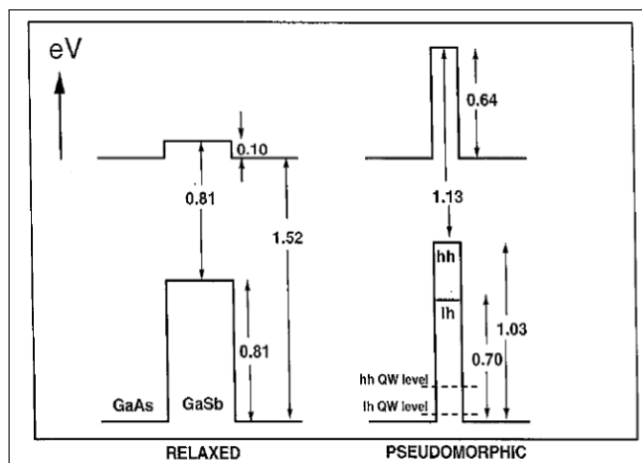


Figure 17

Reference : [7]

Fig. 18 shows PL spectra of three different GaSb/GaAs structures having average GaSb layer thickness 0.3, 0.75 and 1.2 nm. Narrow, sharp and high energy spectrum is observed for low thickness of GaSb layer due to formation of type-II quantum well. However, for more thick GaSb layers, energy becomes lower and spectrum becomes broad due to formation of conventional QDs.

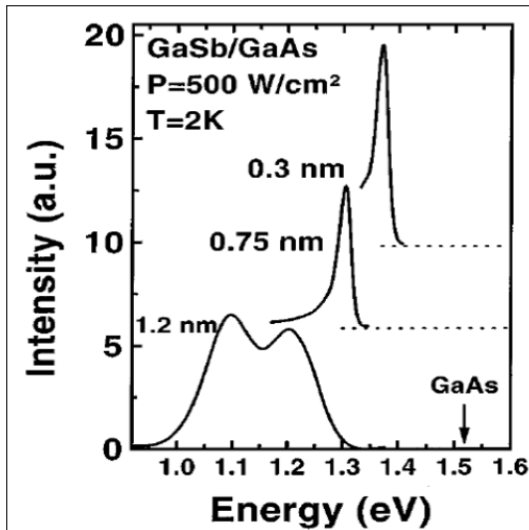


Figure 18
Reference : [7]

Temperature dependence :

The intensity of PL spectra decreases with an increase in temperature and a red shift is observed as well. The lower temperature region is dominated by typical type-I QDs whereas at higher temperatures, the spectrum is dominated by type-II QDs.

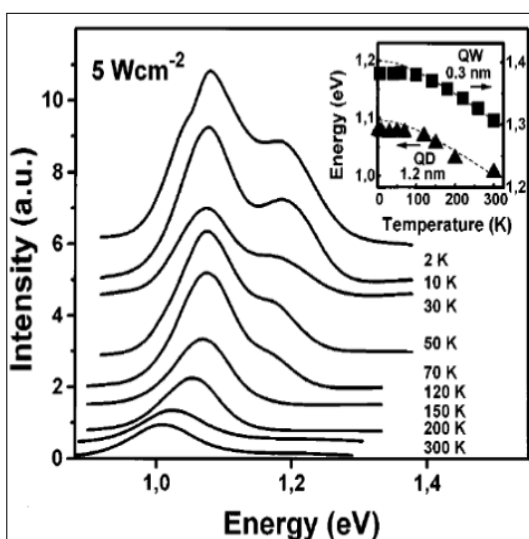


Figure 19
Reference : [7]

IV) Hybrid T2QDs :

Due to their short interband recombination time, type-I QDs might act as recombination centers which makes it difficult to achieve efficiency in InAs/GaAs QD solar cells. Whereas, the spatial separation of electrons and holes in type-II QDs reduces spontaneous recombination. However, it reduces the photon absorption efficiency of type-II QDs as compared to type-I QDs.

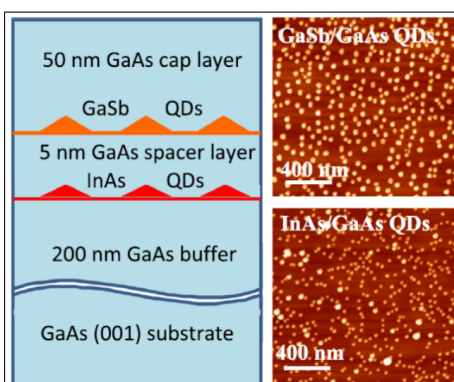


Figure 20

Reference : [9]

It is postulated that GaSb/GaAs QDs can be excellent to the InAs/GaAs solar cell as the formation of InGaAs QWs provides additional absorption. To analyze this, we first grow InAs QDs where a 5nm GaAs spacer is used to cap them. Then, we grow GaSb QDs with 50nm GaAs capping layer. The densities of both QDs are almost similar but the dimensions of GaSb QDs are larger.

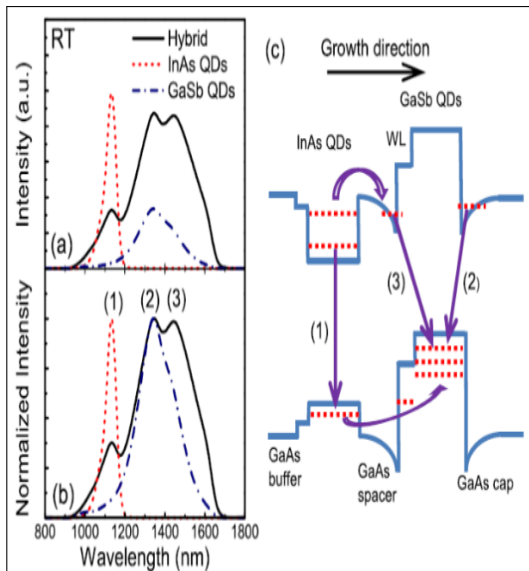


Figure 21

Reference : [9]

To study the PL spectrum, we performed PL measurements at room temperature. Hybrid structure has a broader spectrum as compared to InAs and GaAs QDs. The integrated PL intensity of the hybrid QD sample is 4.1 times higher than the GaSb QD sample and 4.6 times higher than the InAs QD sample, respectively. The hybrid QD structure exhibits a clear enhancement in optical performance and they show promise for creating high efficiency QD solar cells.

Conclusions :

Depending on the application and cost, different types of quantum structure designs are implemented. Innovations have been made in order to improve the systems. T2SL is such a kind of innovation. The unique combination of band structure engineering flexibility and material properties of InAs/GaSb T2SL provides a prospective benefit in the realization of next generation IR imagers. But, despite such promising results, these structures require additional research.

2. Simulation - I

Mid-Wave Infrared InAs/GaSb Type-II Superlattice Photodetector With n-B-p Design Grown on GaAs Substrate

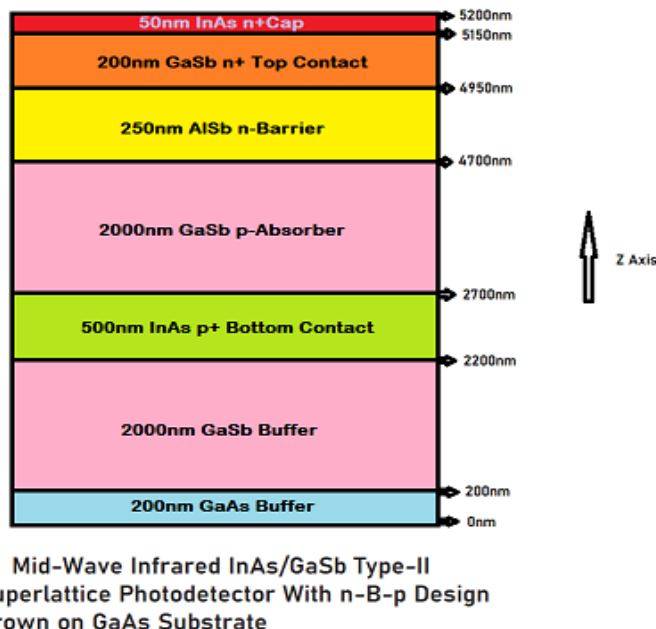


Figure 22

The first simulation I have done is a MWIR InAs/GaSb T2SL photodetector with a unipolar barrier heterostructure, namely the n-B-p architecture on GaAs substrate. The device design consists of an n-type contact, an n-type wide bandgap barrier and a p-type absorber. Similar to the n-B-n design, in n-B-p structure most of the depletion electric field drops across the wide bandgap barrier layer which is designed to reduce the G-R component of dark current. On the other hand, unlike the n-B-n design, in n-B-p variant the n-barrier/p-absorber junction offers a built-in potential, which enables zero-bias operation of the device.

In addition, in n-B-n design the photocurrent is based on minority holes, while in n-B-p structure the p-doped absorber enables the higher mobility electrons to be the minority photocarriers, which is capable to attain higher quantum efficiency.

Simulation Results :

Simulations are performed in nextnano software. The simulations are performed at 77 K.

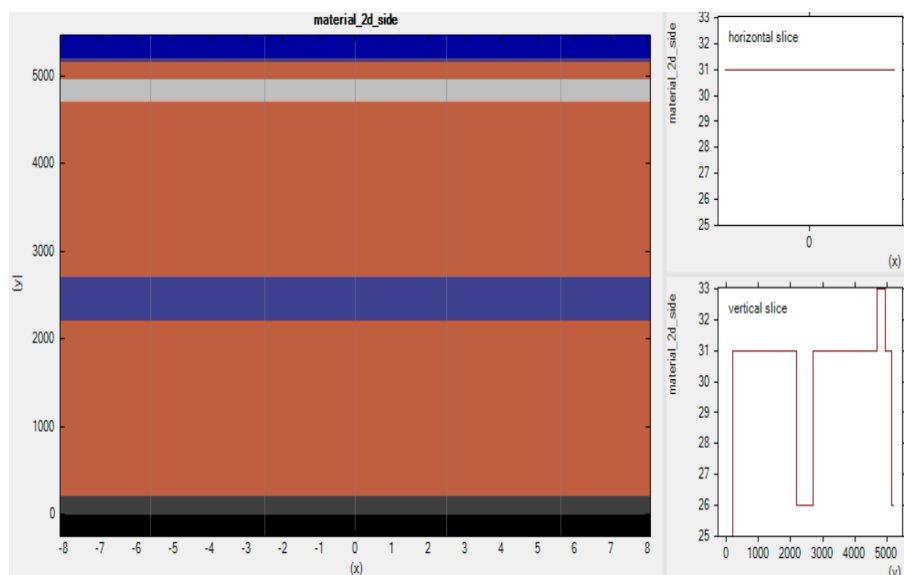


Figure 23 : Material Structure

In Fig. 23, we can notice the material structure of the MWIR InAs/GaSb Type 2 Superlattice Photodetector. Setting the reference value as 0nm of z-axis, 200nm GaAs Buffer extends to 200nm.

Further, 2000nm GaSb Buffer is added from 200nm to 2200nm. Then, 500nm InAs layer is used as p+ Bottom Contact ranging from 2200nm to 2700nm and 2000nm GaAs p-Absorber is added above it upto 4700nm.

Above that, 250nm AlSb n-Barrier is added till 4950nm. Then, n+ Top Contact of 200nm GaSb is added upto 5150nm and finally, 50nm n+ InAs Cap is added upto 5200nm.

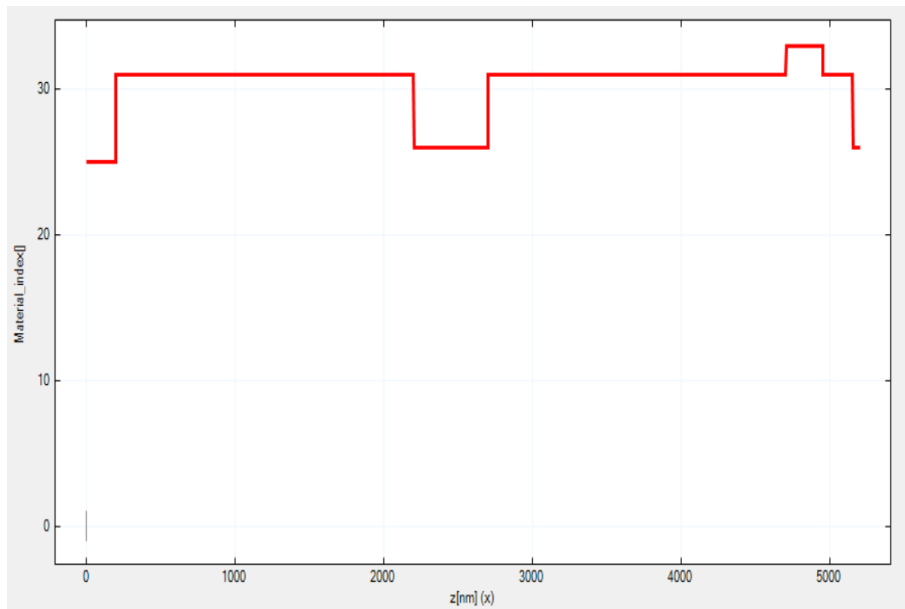


Figure 24 : Material Structure (Z-Axis)

Fig. 24 shows z-axis cross section of material structure of MWIR InAs/GaSb Type 2 Superlattice Photodetector. We can notice that material index changes with change in material.

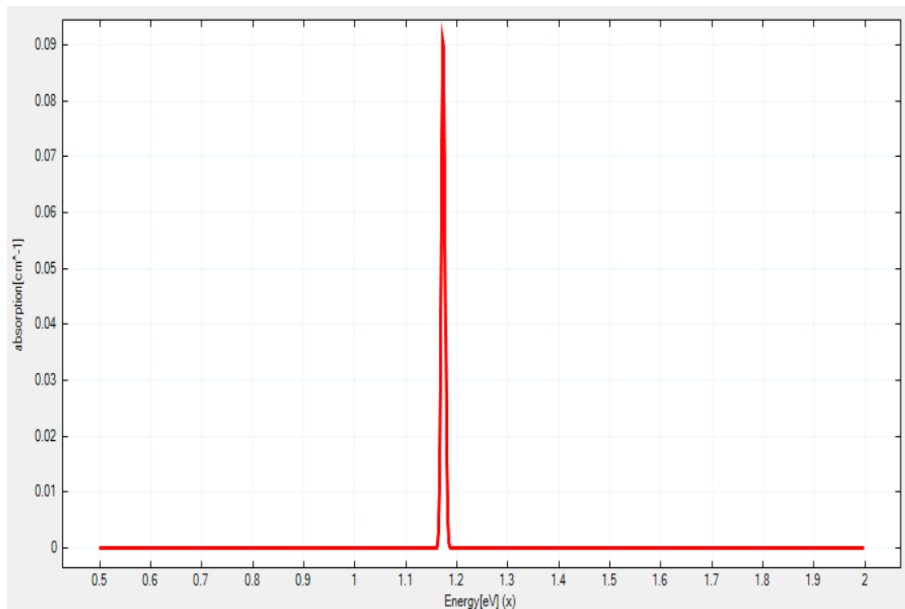


Figure 25 : Absorption Spectrum

Fig. 25 shows the absorption spectrum of MWIR InAs/GaSb Type 2 Superlattice Photodetector. Peak absorption energy is about 12eV which is around 103.3nm as peak absorption wavelength.

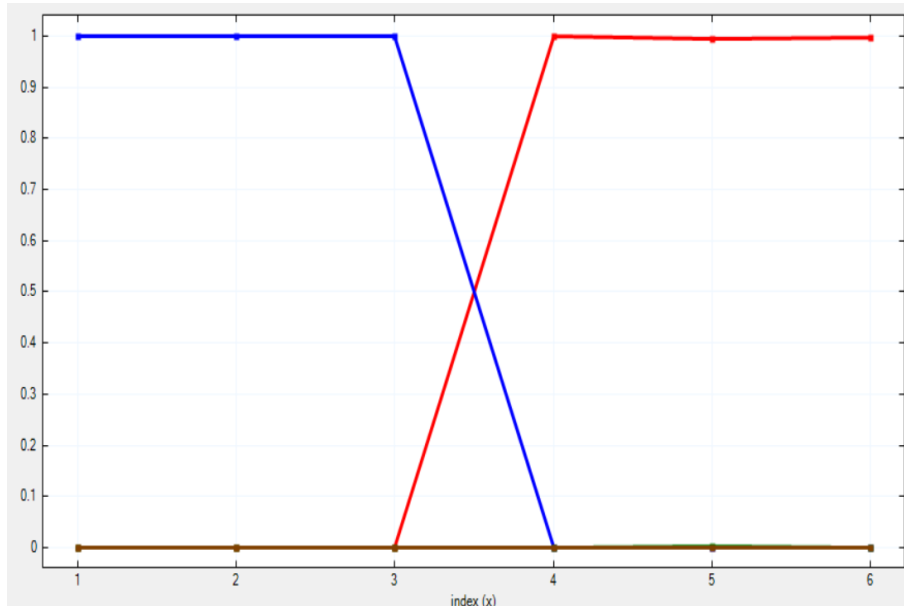


Figure 26 : Component K

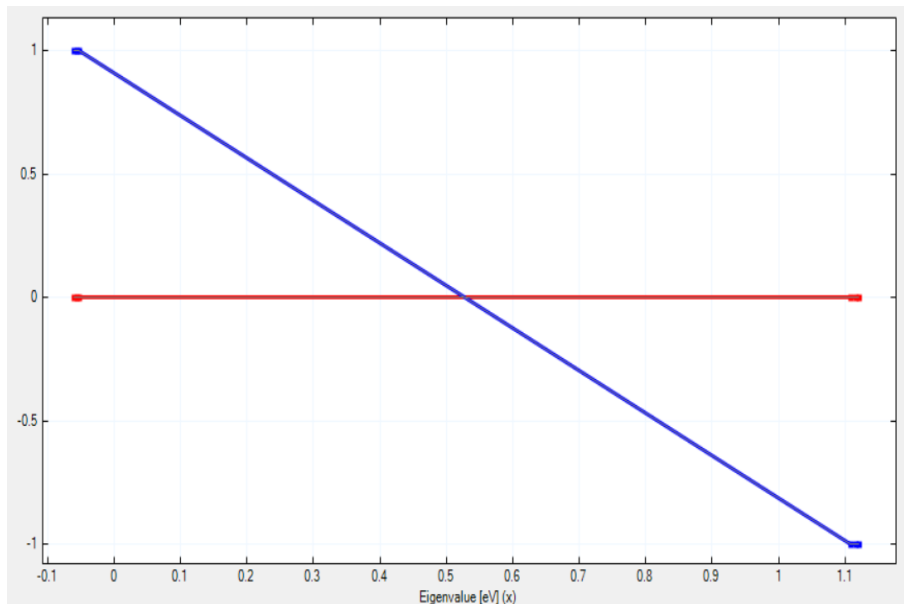


Figure 27 : Eigenvalue Spectrum

Fig. 26 and Fig. 27 show the Component K spectrum and Eigenvalue spectrum of MWIR InAs/GaSb Type 2 Superlattice Photodector.

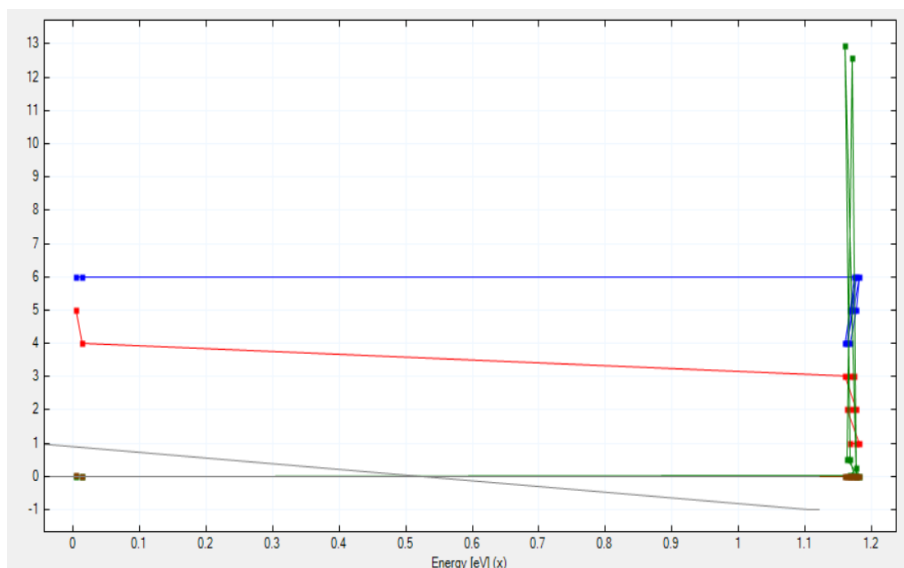


Figure 28 : Transition Spectrum

Transition Spectrum of the structure is shown in Fig. 28. For lower energy values, transitions are much slower as compared to higher energy values.

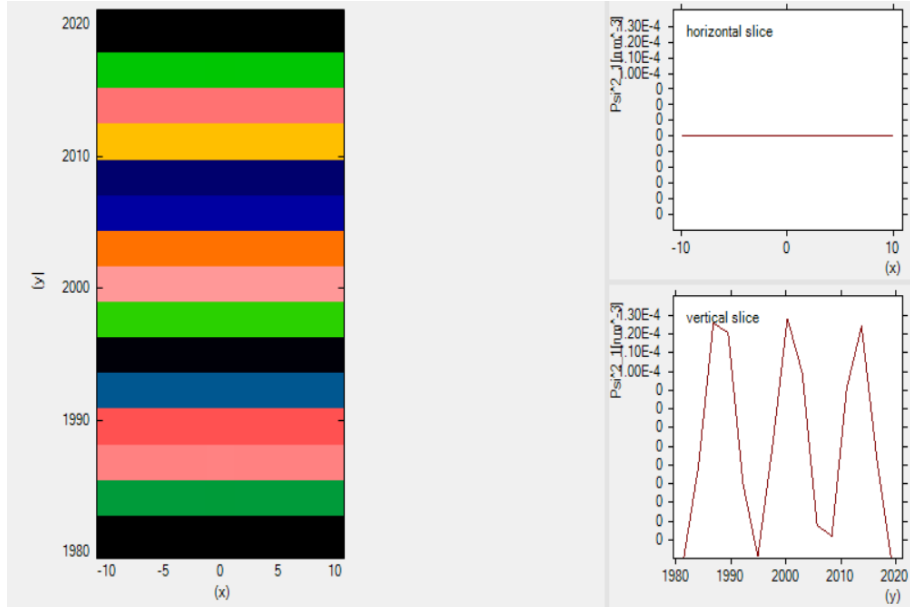


Figure 29 : Dot Probabilities

Fig. 29 shows the dot probabilities of structure along z-axis from 1980nm to 2020nm. There are 3 maximas in the vertical slice where dot probabilities are highest.

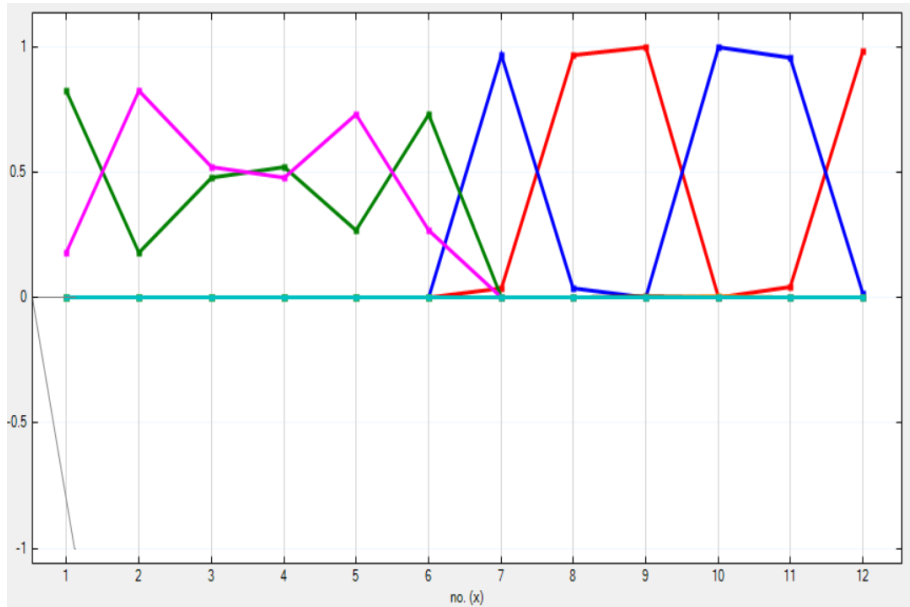


Figure 30 : Spinor Component

Spinor Component Spectrum of MWIR InAs/GaSb Type 2 Superlattice Photodector can be seen in Fig. 30.

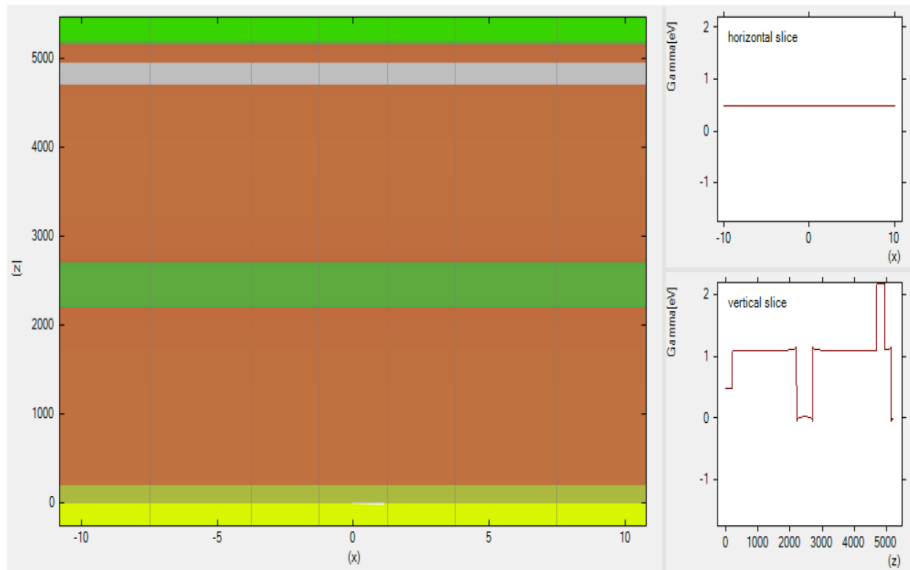


Figure 31 : Band Edges

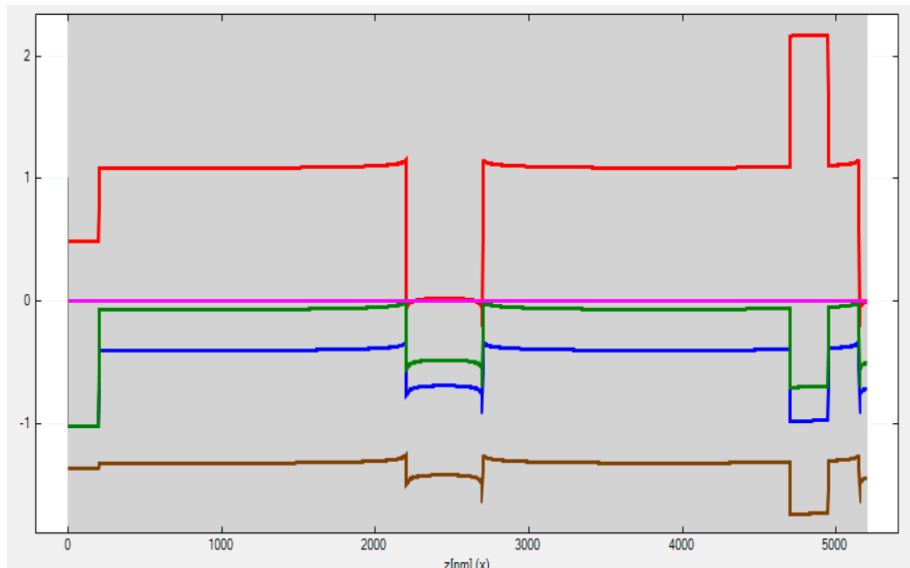


Figure 32 : Band Edges (Z-Axis)

Fig. 31 and Fig. 32 show the bandedges and cross section of bandedges along z-axis of MWIR InAs/GaSb Type 2 Superlattice Photodetector structure. Various bands such as Gamma, LH, HH and SO are shown. Hole fermi energy is around 0eV.

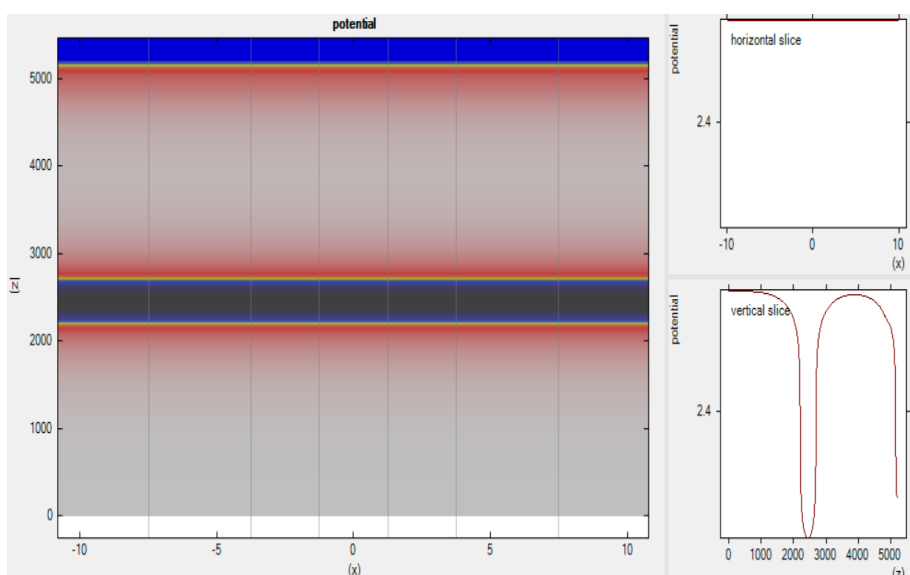


Figure 33 : Potential Plot

Fig. 33 shows the potential plot of MWIR Photodetector Structure. Voltage values in the structure in the vertical section are shown. The minimum voltage is around 2500nm whereas maximum voltage is around 0nm.

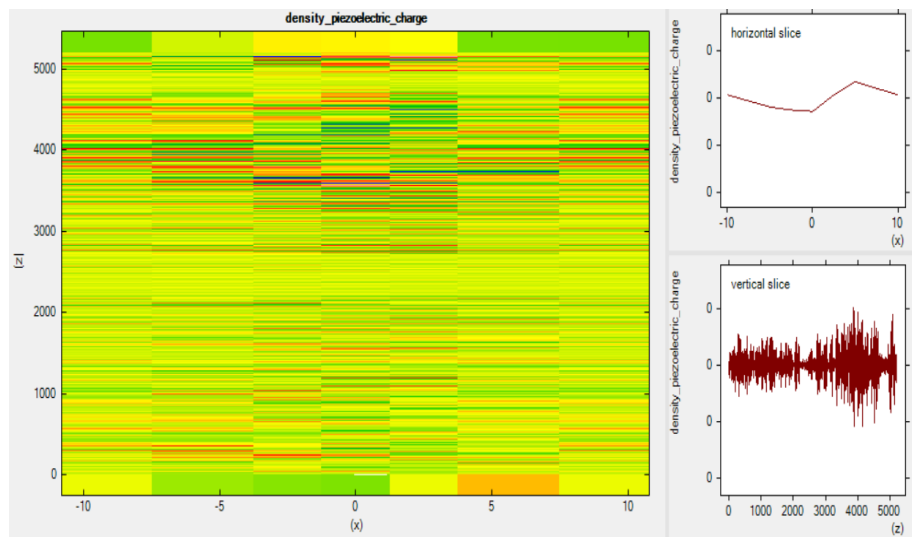


Figure 34 : Piezoelectric Charge Density

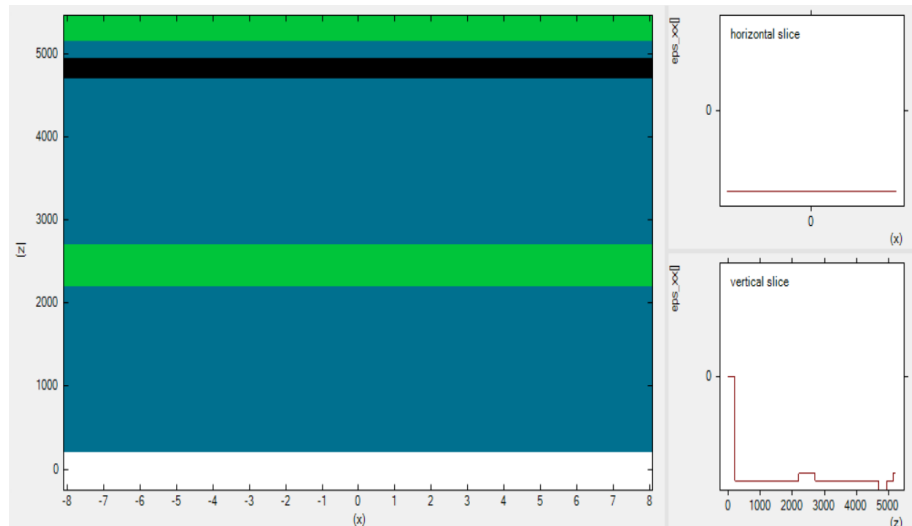


Figure 35 : Strain Simulation

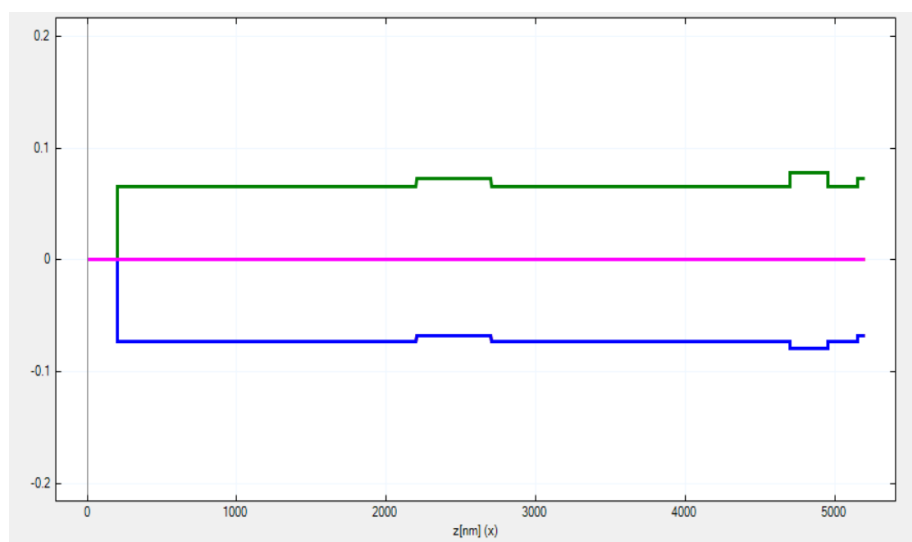
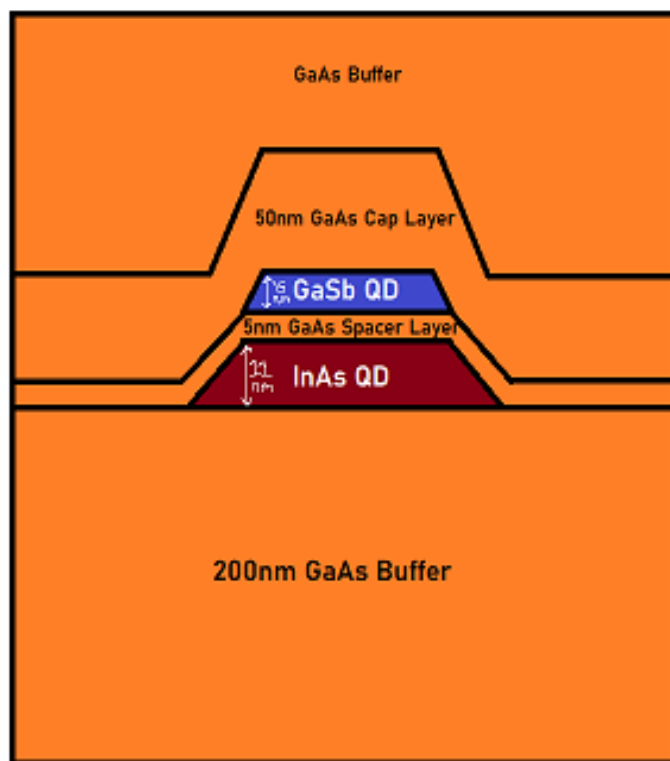


Figure 36 : Strain Simulation (Z-Axis)

Fig. 34, Fig. 35 and Fig. 36 show Piezoelectric Charge Density, Strain Simulation and Strain Vimulation along z-axis respectively. Strain can be seen changing with the change in materials. Strain Curves curves are symmetric about the x-axis.

3. Simulation - II

Hybrid Type-II GaSb/GaAs Quantum Dot Structure



Hybrid type-I InAs/GaAs and type-II GaSb/GaAs quantum dot structure

Figure 37

The structure shown in Fig. 37 is a hybrid type-II GaSb/GaAs quantum dot structure. Two layers of Quantum Dots, InAs (11nm in height) and GaSb (15nm in height) are separated by a 5nm GaAs Spacer Layer.

The spatial separation of electrons and holes in type-II QDs reduces spontaneous recombination, enhancing solar cells' quantum efficiency. But, it reduces the photon absorption efficiency. InAs and GaSb Quantum Dots provide additional absorption.

Simulation Results :

Simulations are performed in nextnano software. The simulations are performed at room temperature (300 K).

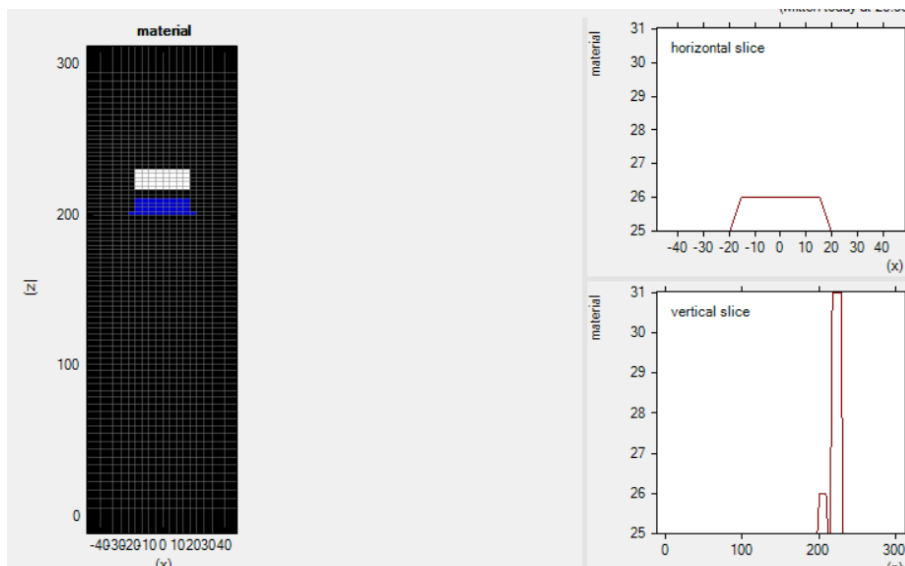


Figure 38 : Material Structure of Type-II Hybrid QD Structure

Fig. 38 shows the material structure of Type 2 Hybrid QD Structure. On the left side, we can clearly notice the two QDs in Blue and White. Black coloured space in the figure is GaAs material. Heights of InAs and GaSb QDs are around 11nm and 15nm respectively.

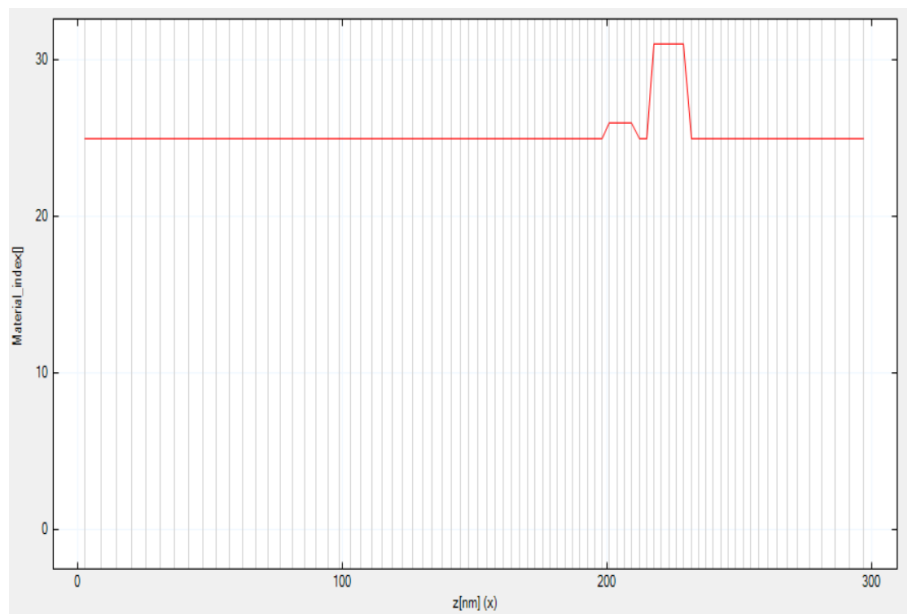


Figure 39 : Material Structure (Z-Axis) of Type-II Hybrid QD Structure

Fig. 39 shows the z-axis cross-section of material structure of Type 2 Hybrid QD Structure. We can clearly notice the change in the material index at QDs.

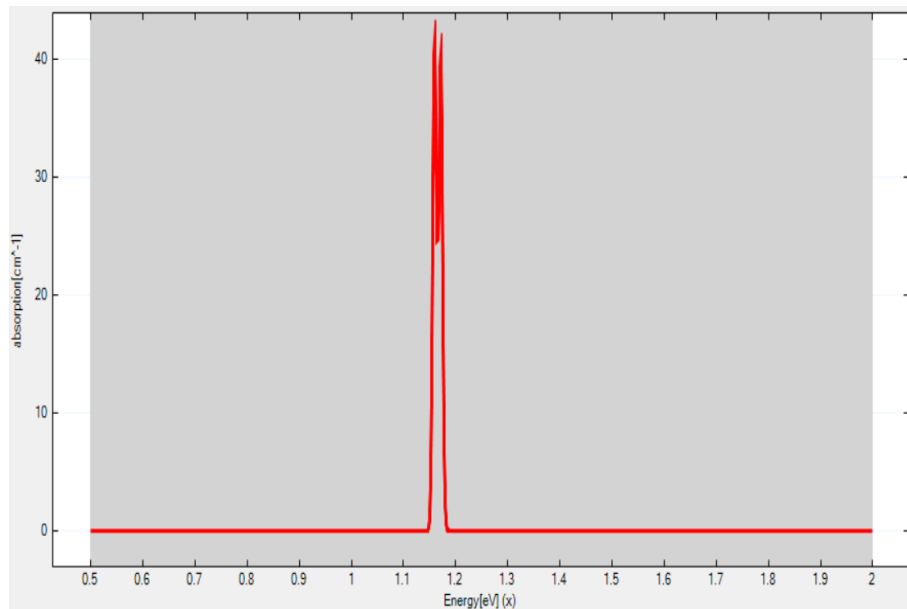


Figure 40 : Absorption Spectrum of Type-II Hybrid QD Structure

The absorption spectrum of Type II Hybrid QD Structure can be seen in Fig. 40. Because of the presence of 2 QDs of different materials, 2 spikes can be seen in the absorption spectrum.

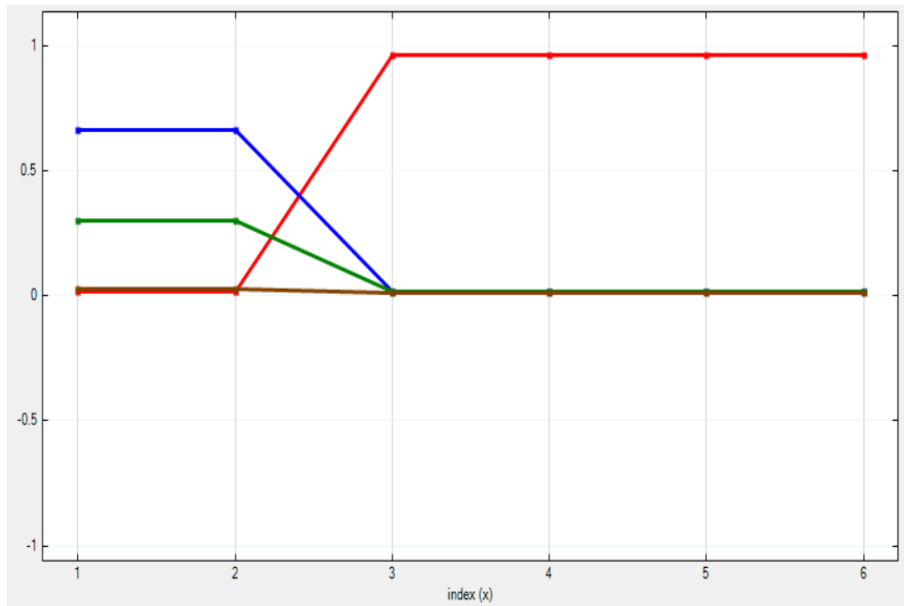


Figure 41 : Component K of Type-II Hybrid QD Structure

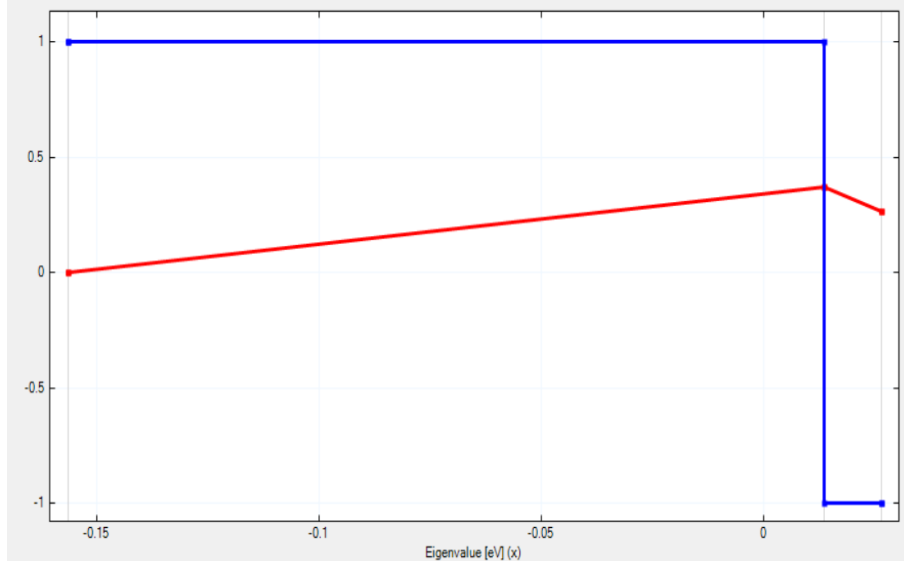


Figure 42 : Eigenvalue Spectrum of Type-II Hybrid QD Structure

Fig. 41 and Fig. 42 show the Component K spectrum and Eigenvalue spectrum of Type II Hybrid QD Structure.

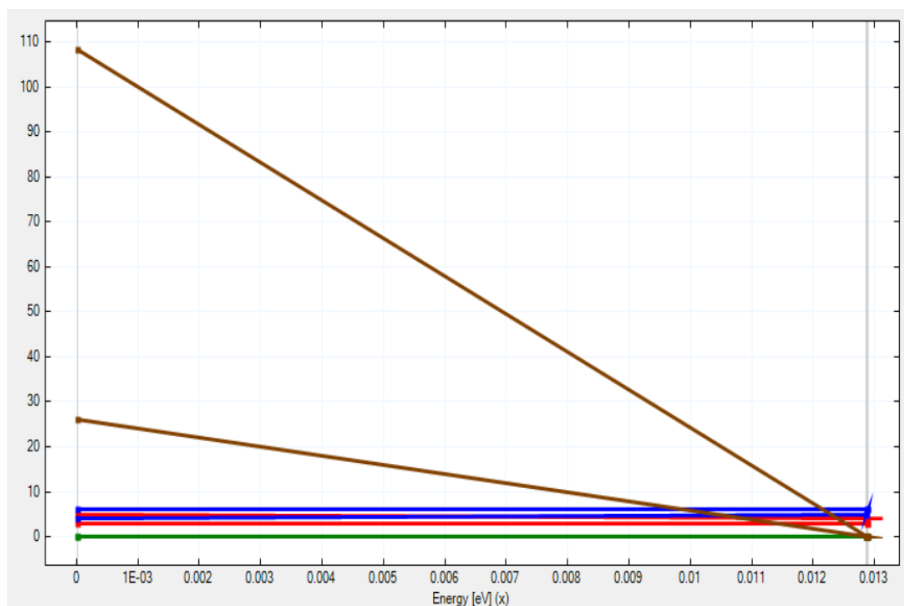


Figure 43 : Transition Spectrum of Type-II Hybrid QD Structure

Transition Spectrum of Type II Hybrid QDs can be seen in Fig. 43. With the increase in energy, transitions come closer as compared to lower energy levels.

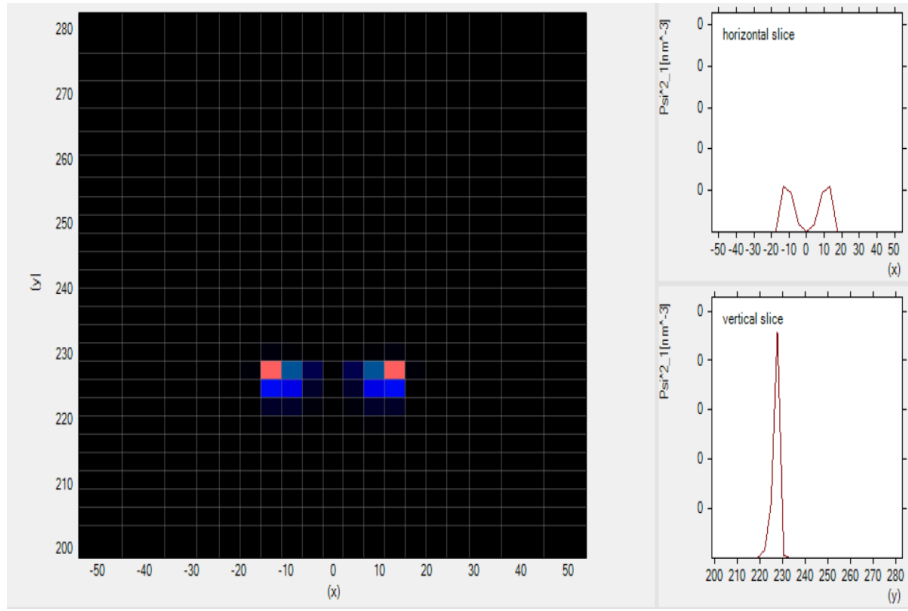


Figure 44 : Dot Probabilities of Type-II Hybrid QD Structure

Dot probabilities of the structure is shown in Fig. 44. In the horizontal direction, dot probability is highest along the QDs whereas, in the vertical direction, dot probability is highest between the two QDs.

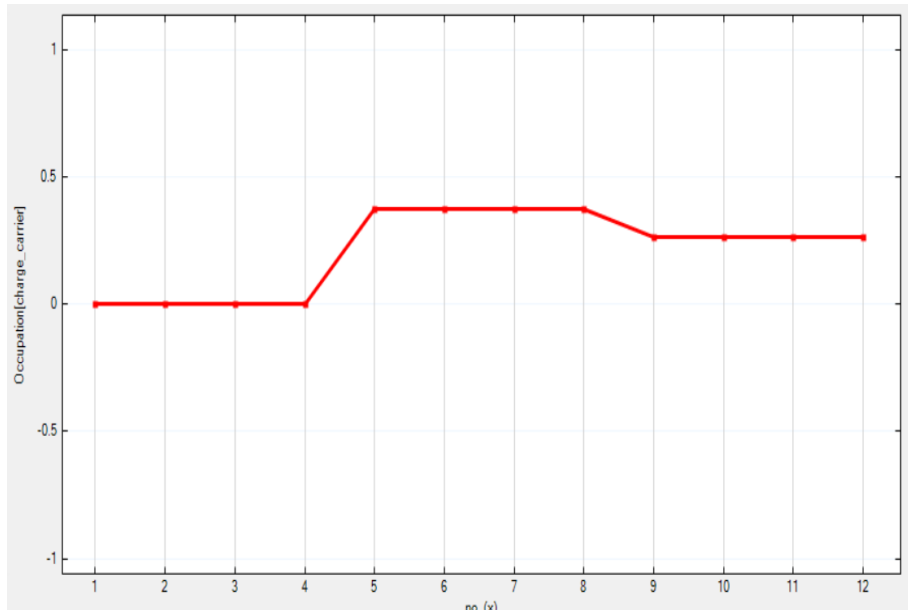


Figure 45 : Dot Occupancy of Type-II Hybrid QD Structure

Fig. 45 shows the dot occupancy of Type II Hybrid QD structure.

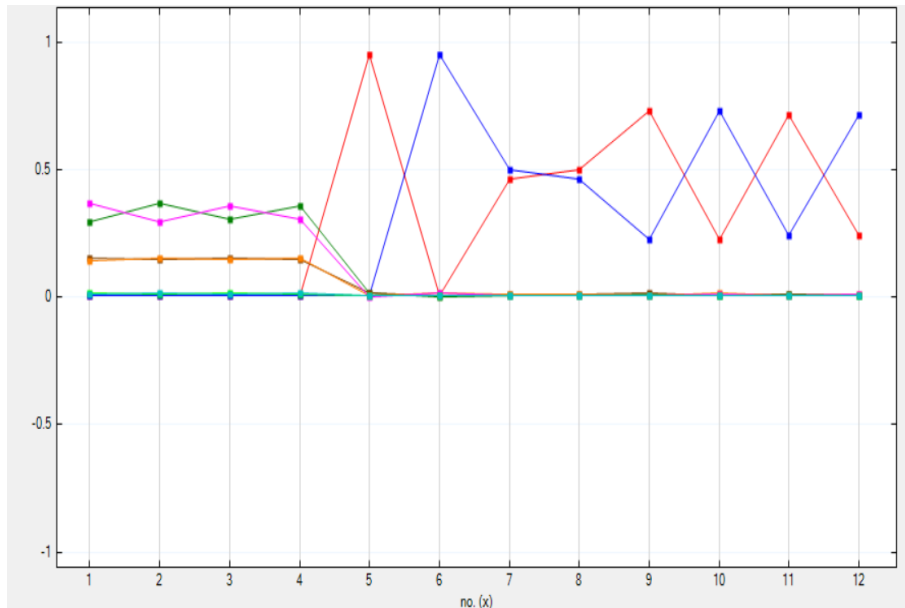


Figure 46 : Spinor Component of Type-II Hybrid QD Structure

Spinor Component Spectrum of Type 2 Hybrid Quantum Dot Structure can be seen in Fig. 46.

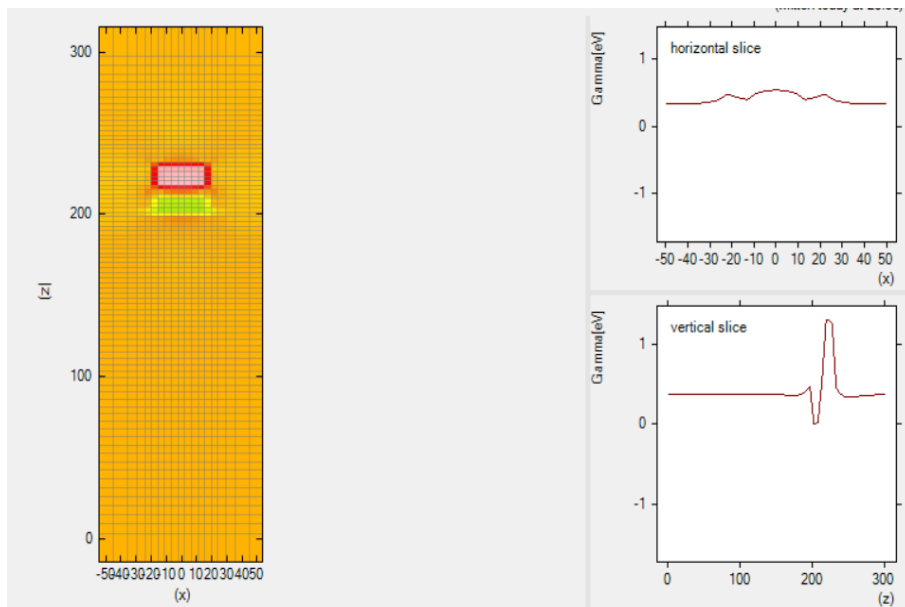


Figure 47 : Band Edges of Type-II Hybrid QD Structure

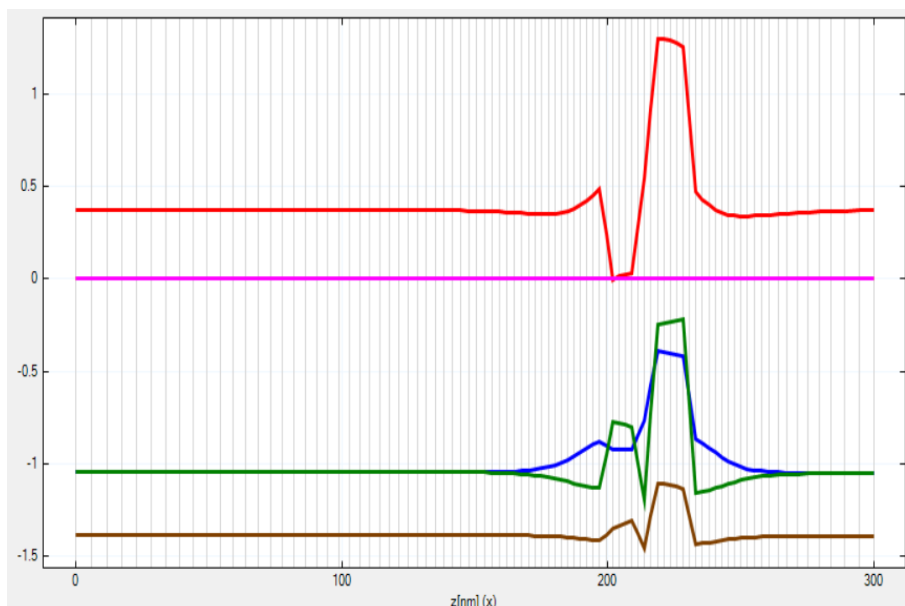


Figure 48 : Band Edges (Z-Axis) of Type-II Hybrid QD Structure

Fig. 47 and Fig. 48 shows the band edges of Type II Hybrid QD structure. All types of bands such as Gamma, LH, HH and SO are shown. Horizontal slice slows spikes around the QDs. Hole as well as electron fermi energies are shown as well.

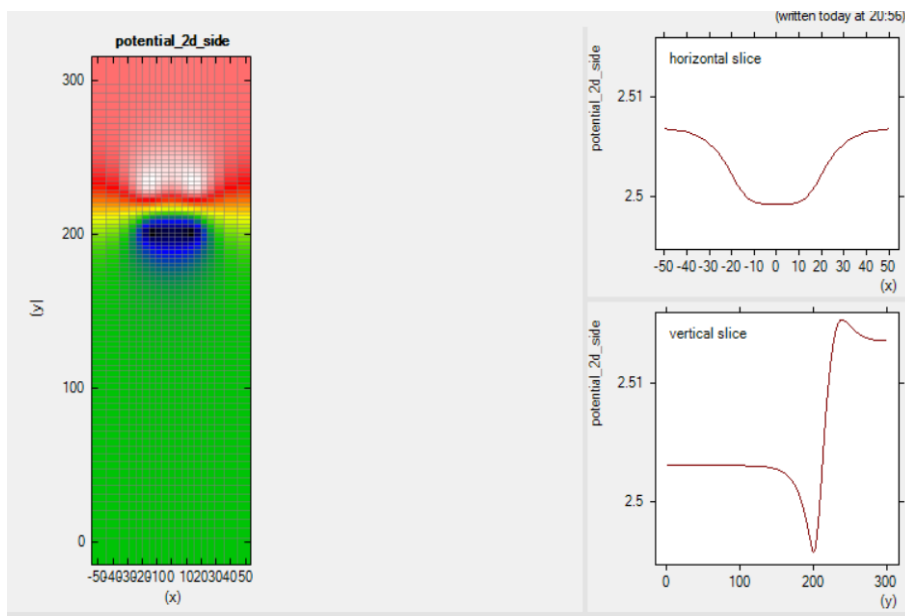


Figure 49 : Potential Plot of Type-II Hybrid QD Structure

Potential Plot of the structure is shown in Fig. 49. In the vertical direction, potential decreases and reaches to its minimum value in the first QD. Then, it increases and reaches its peak in the second QD.

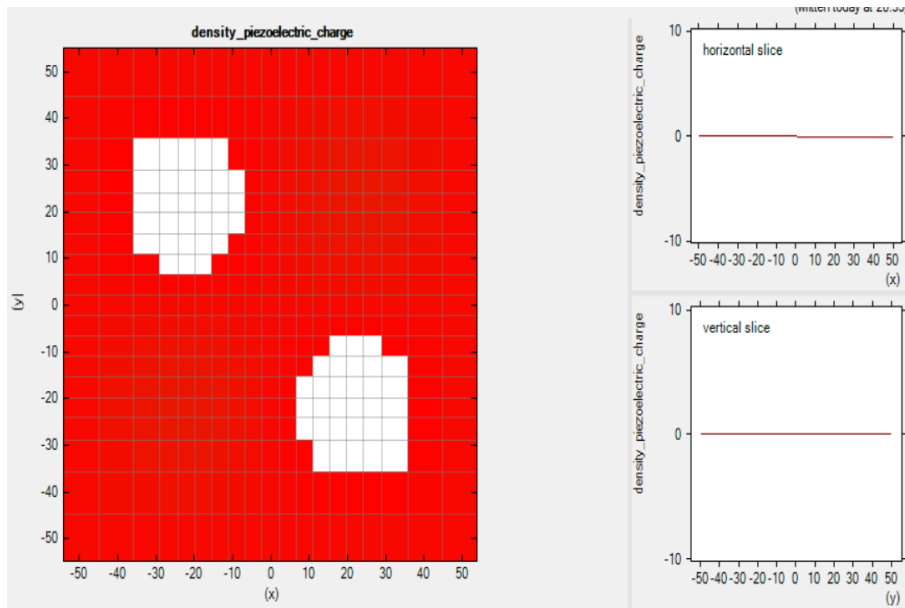


Figure 50 : Piezoelectric Charge Density (XY-Plane) of Type-II Hybrid QD Structure

Piezoelectric Charge Density around XY Plane of Type II Hybrid QD Structure is shown in Fig. 50.

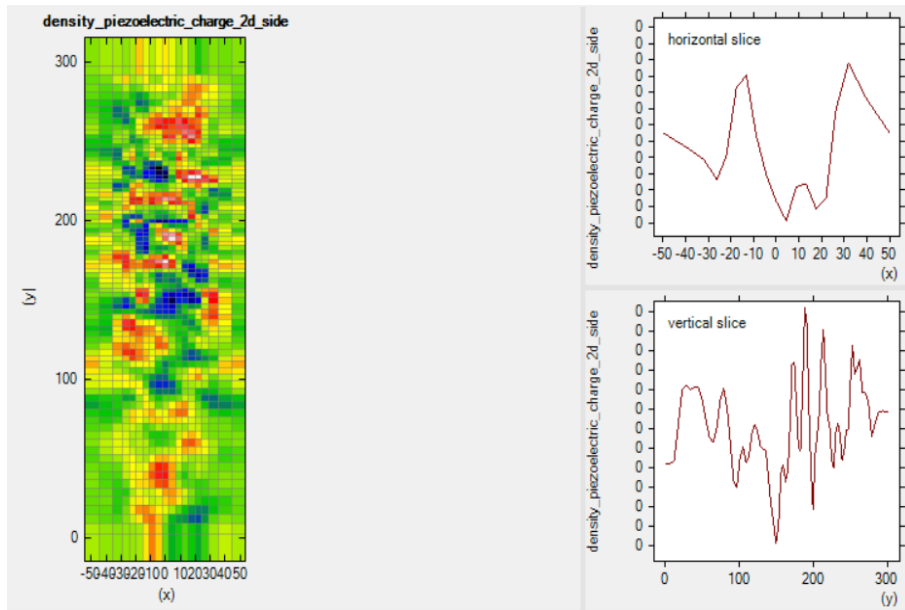


Figure 51 : Piezoelectric Charge Density (XZ-Plane) of Type-II Hybrid QD Structure

Piezoelectric Charge Density around XZ Plane of Type II Hybrid QD Structure is shown in Fig. 51 which is more random as compared to XY Plane.

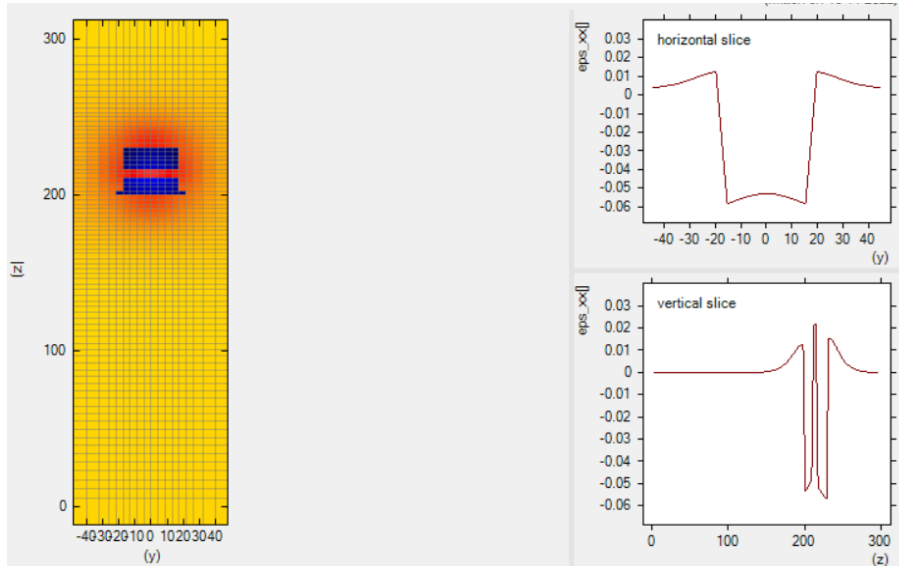


Figure 52 : Strain Simulation of Type-II Hybrid QD Structure

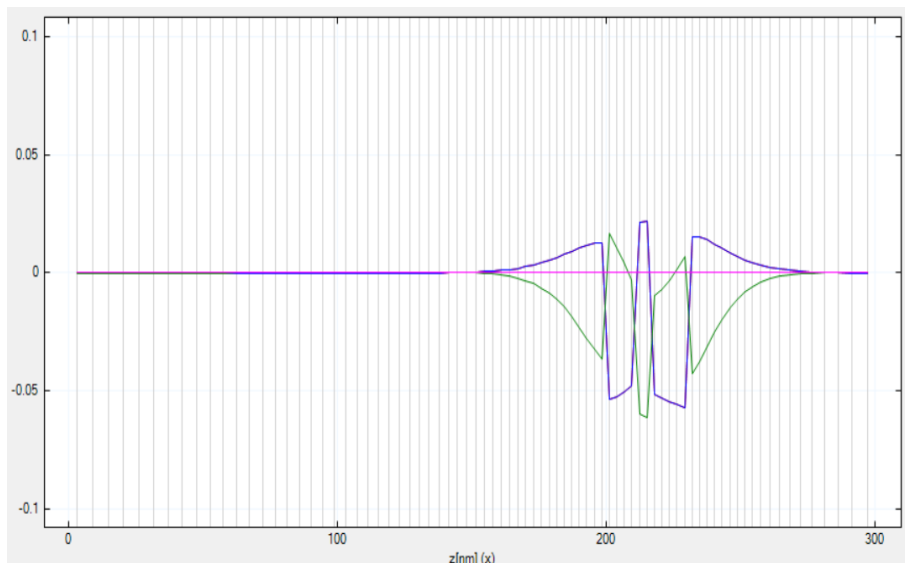


Figure 53 : Strain Simulation (Z-Axis) of Type-II Hybrid QD Structure

Fig. 52 and Fig. 53 show Strain Simulation and vertical slice of Strain Simulation of Type II Hybrid QD Structure respectively. In the vertical direction, strain is lowest within the QDs but its peak is between the QDs. Whereas, in the horizontal direction, strain is lowest at the QDs.

4. Appendix

The code files used to generate the results and other resources are in the GitHub repository link : <https://github.com/MayurWare/EE451-SRE>

5. References

References :

- [1] Elena A. Plis, "InAs/GaSb Type-II Superlattice Detectors", Advances in Electronics, Vol. 2014 (2014)
- [2] A. Rogalski, "Insight on quantum dot infrared photodetectors", 2nd National Conference on Nanotechnology 'NANO 2008', Vol. 146 (2009)
- [3] Amir Karim and Jan Y Andersson, "Infrared detectors:Advances, challenges and new technologies", IOP Conf. Series : Materials Science and Engineering Vol. 51 (2013)
- [4] B-M. Nguyen, M. Razeghi, V. Nathan, Gail J. Brown, "Type-II M structure photodiodes: an alternative material design for mid-wave to long wavelength infrared regimes," Proc. SPIE 6479, Quantum Sensing and Nanophotonic Devices IV, 64790S (21 February 2007)
- [5] Zhuo Deng , Daqian Guo, "Mid-Wave Infrared InAs/GaSb Type-II Superlattice Photodetector With n-B-p Design Grown on GaAs Substrate", IEEE JOURNAL OF QUANTUM ELECTRONICS, VOL. 55, NO. 4 (August 2019)
- [6] E. R. Glaser, B. R. Bennett, B. V. Shanabrook, and R. Magno, "Photoluminescence studies of selfassembled InSb, GaSb, and AlSb quantum dot heterostructures", Appl. Phys. Lett., Vol. 68, No. 25, 17 June 1996
- [7] F. Hatami, N. N. Ledentsov, M. Grundmann, J. Böhrer, F. Heinrichsdorff, "Radiative recombination in typeII GaSb/GaAs quantum dots", Appl. Phys. Lett., Vol. 67, No. 5, 31 July 1995
- [8] Adrienne D. Stiff-Roberts, "Quantum-dot infrared photodetectors: a review", Journal of Nanophotonics, Vol. 3, 031607 (14 April 2009)
- [9] Hai-Ming Ji, Baolai Liang, Paul J. Simmonds, "Hybrid type-I InAs/GaAs and type-II GaSb/GaAs quantum dot structure with enhanced photoluminescence", APPLIED PHYSICS LETTERS 106, 103104 (2015)
- [10] <https://en.wikipedia.com>
- [11] Nextnano Online Documentation - <https://www.nextnano.com/dokuwiki/doku.php>

